Welding in the World (2022) 66:731–744
https://doi.org/10.1007/s40194-021-01237-6

RESEARCH PAPER

On the interaction of axial and bending loads in the weld root fatigue strength assessment of load-carrying cruciform joints

Antti Ahola[1] · **Rohani Raftar Hamidreza**[1] · **Timo Björk**[1] · **Olavi Kukkonen**[1]

Received: 3 September 2021 / Accepted: 13 December 2021 / Published online: 21 January 2022

Abstract

Current design standards and recommendations incorporate the nominal stress system for assessing the fatigue strength capacity of load-carrying cruciform (LCX) joints with the fillet welds and failing from the weld root. Thus far, bending-loaded joints have not been addressed in these standards. The aim of the present study is to investigate the fatigue performance of LCX joints subjected to cyclic axial and bending loads. Firstly, fatigue test data sets of such joints subjected to axial loading and bending loads in the adjoined plate component are extracted from the literature, and statistical analyses are carried out to evaluate the fatigue strength capacity using the nominal weld stresses (NWSs). Secondly, experimental fatigue tests are carried out on LCX joints made of ultra-high-strength steel (UHSS) grade using constant amplitude loading and subjected to combined axial and bending load to study the load interaction effects on the fatigue strength capacity. The results showed that the FAT36 detail category for the weld root failures is applicable for bending-loaded joints when applying NWSs calculated on the basis of effective throat thickness of weld and assuming linear-elastic stress distribution over the joint section. The effective notch stress analyses showed unconservative results for the tested joints, when applying FAT225 design curve with the reference radius of $r_{ref} = 1.0$ mm.

Keywords Fatigue · Welded joint · Cruciform joint · Weld root · Bending · Ultra-high-strength steel

1 Introduction

In fillet weld joints subjected to cyclic loads at the adjoined plate component, i.e., load-carrying T-joints or load-carrying cruciform (LCX) joints, the infusible weld root acts as an initial crack for the fatigue crack propagation. Therefore, the weld root fatigue strength is amongst the most important fatigue design criteria in such joints. In the fatigue design of LCX joints, weld sizing and groove preparation, share of secondary bending stresses, and post-weld treatments are the key factors influencing fatigue strength capacity and failure location [1–5]. The analytical approach, referring to the nominal stress approach, is an elementary but efficient method for assessing weld root fatigue strength capacity — the nominal weld stresses (NWSs) can be calculated using the load components at the adjoined plate members. However, current design codes and standards [6–9] cover the analytical model only for the fillet-welded LCX joints subjected to axial loads, and far too little attention has been paid to LCX joints subjected to bending loads.

Ghafoori-Ahangar and Verreman [10] evaluated the fatigue strength of LCX joints made of stainless steel grades under three-point bending and Mori et al. [11, 12] fatigue-tested LCX joints made of a mild structural steel grade. In both studies, the ligament size (weld size and penetration) was found as an important factor influencing the weld root fatigue performance under bending. Nevertheless, no proposals were given in these studies for applying NWSs in fatigue strength assessments. Meanwhile, great efforts have been done to verify the fatigue analysis methodologies for assessing the weld root failures of cruciform joint using various local approaches, such as effective notch stress (ENS) concepts [13–15], structural stress approaches [16–18], notch stress intensity factor (NSIF)-based peak stress method [19], and strain energy density method [4, 20], and applying

Recommended for publication by Commission XIII - Fatigue of Welded Components and Structures

✉ Antti Ahola
antti.ahola@lut.fi

[1] Laboratory of Steel Structures, Lappeenranta-Lahti University of Technology LUT, P.O. Box 20, FI-53851 Lappeenranta, Finland

the theory of critical distance (TCD) [14, 21]. Although the local approaches can provide substantial improvement in the accuracy of fatigue assessments, the nominal stress method is still widely used in engineering and important at least for preliminary analyses.

To the authors' knowledge, an analytical model for bending-loaded LC fillet weld joints has been suggested in the upcoming revision of the Eurocode 3 (EC3) fatigue design standard, aiming on the introduction of the analytical model in the upcoming revision of the EN 1993–1-9 standard [6]. Nevertheless, this model still lacks experimental validation, and this work aims to verify different models for assessing weld root failures using NWSs. In a previous work [22], an analytical method, different to the new model proposed in the final draft of the new revision of EC3, parts 1–9 [6], for calculating NWSs under bending loading, was proposed using the limited number of experimental fatigue test data. The results showed in accordance with the FAT36 design curve applied in association with the nominal stress approach. In the proposed model, the NWSs are calculated using a linear-elastic stress distribution over the joint section. Despite of these encouraging results, more experimental verifications for the findings are needed. In addition, the prior experimental and numerical investigations have indicated that the crack growth path starting from the weld root in the axial loading is different in axial loading to the behavior in the bending loading — for the bending-loaded joints, the crack path is curved at the leg section, while for the axially loaded joints, crack path is more straight and turns 10–20 °C towards the throat section, as also demonstrated in Fig. 1 by numerical and experimental results. Similar differences in crack paths for joints under axial and bending loads have been also demonstrated in previous works dealing with LCX joints with root failures; see, e.g., [10–12, 23]. Based on the crack propagation analysis, the different crack paths can be explained by the stress field at the weld root, and the crack path corresponds to the maximum principle stress direction. Due to these differences, the interaction of axial and bending loads cannot be considered by the superposition principle to calculate NWSs under combined cyclic axial and bending loads, and the interaction effects should be studied more in detail. For instance, Anami et al. [24] found that an additional 25% bending stress to axial membrane stress did not majorly decrease the fatigue strength capacity of LC joints compared to the joints subjected to pure axial loading.

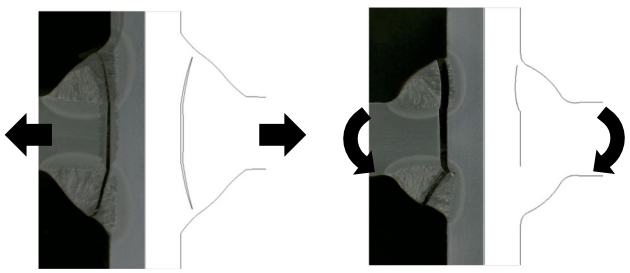

Fig. 1 Fatigue fracture paths from the weld root in the LCX joints subjected to axial and bending loads, determined by an experimental fatigue test (left) and a numerical crack growth analysis (right) [25]

The aim of the present study is to collect the fatigue test data to evaluate the applicability of the proposed models for calculating NWSs in bending-loaded LCX joints, i.e., the force-pair model suggested by the working group of the EC3 revision, and the model proposed by the authors in their prior investigation; see Sect. 2. Furthermore, experimental fatigue tests are carried out for the LCX joints made of S960 UHSS grade to investigate the interaction of axial and bending loading. The specimens are fabricated with angular misalignment to introduce secondary bending stress with the degree of bending (DOB $= \sigma_b/(\sigma_m + \sigma_b)$, where σ_b and σ_m are the bending and membrane stress, respectively, at the plate component) of DOB = 0.25 and DOB = 0.6. This part of the study is described in Sect. 3. Section 4 introduces the analysis of ENSs of LCX joints at the weld root, which are obtained under different load components using numerical finite element (FE) modeling with the reference radius of $r_{ref} = 1.0$ mm [26, 27].

2 Overview on existing experimental fatigue test data

2.1 Axial loading

Axial fatigue tests are usually easier to perform, and on the other hand, bending loads are regarded to produce higher fatigue strength than axial loads. Therefore, fatigue design *S–N* curves have been established using fatigue test data of axial loads [28, 29]. For weld root failures in LC joints, FAT36 or FAT40 (depending on the throat thickness to plate thickness, *a*/*t*, ratio) is widely provided in design guidelines, and NWS range can be formulated simply (see also Fig. 2a) assuming welds with equal throat size:

$$\Delta\sigma_{w,m} = \frac{\Delta F}{2a_{eff}} = \frac{\Delta\sigma_m t}{2a_{eff}}, \quad (1)$$

where ΔF is the unit force range (force/length), a_{eff} is the effective throat thickness, and $\Delta\sigma_m$ is the membrane stress at the plate component. In the prior investigation [22], fracture mechanics-based analysis showed that the weld root fatigue strength improvement gained by weld penetration refers to external throat thickness summed with weld penetration depth, p (see also dimensions shown in Fig. 2b) in the axially loaded cruciform joints. Based on this observation, the NWS under the axial loading could be obtained based on the following equation:

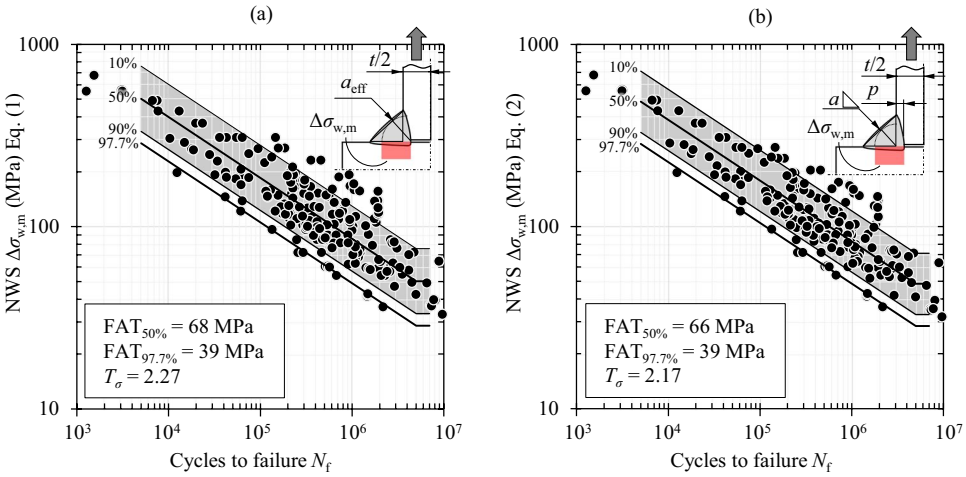

Fig. 2 Fatigue test data (see Appendix Table 6) of axially loaded LCX joints evaluated using the nominal stress approach ($m=3$) — NWSs calculated based on the **a** effective throat thickness and **b** external weld throat thickness and weld penetration, data from [3–5, 12, 17, 22, 24, 30–42]

$$\Delta\sigma_{w,m} = \frac{\Delta F}{2(a+p)} = \frac{\Delta\sigma_m t}{2(a+p)}. \quad (2)$$

Rohani Raftar et al. [13] re-evaluated the fatigue test data of LC joints with the weld root failures and evaluated the fatigue strength with the ENS approach using various radii. Applying the extracted data, Fig. 2 presents the fatigue test data in terms of the NWSs applying both ligament sizes — effective weld throat thickness (a_{eff}) and external weld throat thickness summed with weld penetration ($a+p$) as per Eqs. (1) and (2). It is worth mentioning that the extracted data only comprises data sets in which weld sizes and penetrations were reported (e.g., by macrographs) to correctly account for the ligament sizes in the calculation of NWSs. Studies, in which only the external throat thicknesses were reported, were excluded from this analysis. The *S*–*N* data analyses were carried out using the standard statistical evaluation procedure [7], i.e., *S* as an independent (known) variable, and *N* as a dependent (unknown) variable, using both a fixed slope parameter ($m=3$), and free curve fitting (m_{free}) due to the high number of data points extracted for the analysis. The characteristic design curves were obtained as follows:

$$\log C = \log N_f + m\log\Delta\sigma, \quad (3)$$

$$C_{char} = C_{mean} - k \cdot \mathrm{Stdv}, \quad (4)$$

where the characteristic factor k is:

$$k = 1.645 \cdot \left(1 + \frac{1}{\sqrt{n}}\right), \quad (5)$$

and C is the fatigue capacity (characteristic (char) with a survival probability of $P_s=97.7\%$ or, mean, $P_s=50\%$), Stdv is the standard deviation, and n is the number of data points.

2.2 Bending loading

As discussed in Sect. 1, weld root fatigue strength capacity under the plate out-of-plane plate bending loading has not been extensively studied in prior investigations. However, through experimental verification, the use of linear-elastic stress distribution over the joint section was proposed [22], and NWS can be calculated as follows (Fig. 3a):

$$\Delta\sigma_{w,b} = \frac{\Delta M c}{I} = \frac{\Delta\sigma_b \frac{t^2}{6}\frac{w}{2}}{\frac{(w+2a_{eff})^3 - w^3}{12}} = \frac{\Delta\sigma_b t^2 w}{6w^2 a_{eff} + 12 w {a_{eff}}^2 + 8{a_{eff}}^3}, \quad (6)$$

where ΔM is the plate moment range, c is the distance from the neutral axis to weld root ($=w/2$), I is the section modulus, and w is the infusible weld root length. The experimental results evaluated using the proposed equation showed correspondence with the FAT36 design curve [22]. A simpler model, corresponding to the force pair acting at the welds, provides uniform stress over the weld size at the transverse leg section (Fig. 3b). To the authors knowledge, this model has been suggested for calculating NWSs in the bending-loaded joints in the new EC3 1–9 revision as per the final draft [43] and related working group discussions. When employing the force-pair model, the NWS is computed as follows:

$$\Delta\sigma_{w,b} = \frac{\Delta F_w}{a_{eff}} = \frac{\Delta M}{a_{eff}\left(a_{eff}+w\right)} = \frac{\Delta\sigma_b t^2}{6a_{eff}\left(a_{eff}+w\right)}, \quad (7)$$

where ΔF_w is the unit force range at the weld (force/length, as the weld stress is independent of the weld length in the case of continuous fillet weld). It is worth mentioning that for the fatigue design purposes, zero weld penetration should be assumed, i.e., $w=t$ and $a=a_{eff}$. However, Eqs. (6) and (7) for the bending loads, as well as Eqs. (1) and (2)

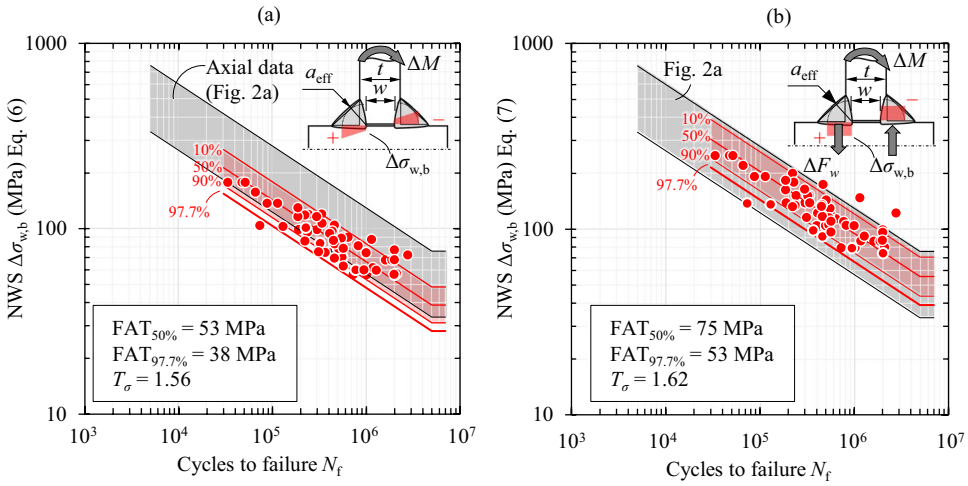

Fig. 3 Fatigue test data (see Appendix Table 7) of bending-loaded LCX joints evaluated using the nominal stress approach ($m=3$) — NWSs calculated based on the (**a**) linear-elastic stress distribution over the joint section and (**b**) force pair system, data from [10–12, 22, 23]

for the axial loads, are applied to evaluate the fatigue test results, and it is conservative to consider the weld penetration (results in lower stresses and fatigue strengths). This is important particularly in the bending-loaded joints. To evaluate the applicability of these two proposals, experimental data is acquired from the published literature data, and data plots with the obtained scatter bands, together with the *S*–*N* curves, have been presented in Fig. 3 for both models. Table 1 summarizes the results of the statistical analyses for both axially loaded and bending-loaded LCX joints, showing the fatigue strengths and scatter range indexes obtained using both a fixed slope, $m=3$, and free slope, m_{free}.

3 Experiments

3.1 Materials

The study continues the experimental work carried out in [22] with new tests on the interaction loads, and thus S960MC UHSS grade with the plate thickness of $t=9$ mm was chosen for this study. The welded joints were prepared with gas metal arc welding (GMAW) using a strength-matching filler metal, Böhler Union X96 [44, 45] (nominally under-matching). The chemical composition and mechanical properties of the studied materials have been presented in Tables 2 and 3, respectively.

Table 1 Summary on the results of the statistical analysis carried out for the fatigue test data of LCX under axial and bending loading in the nominal stress system (see also Figs. 2 and 3)

Loading type	NWS model		Fig.	$m=3$			m_{free}			
				$FAT_{50\%}$ (MPa)	$FAT_{97.7\%}$ (MPa)	T_σ (-)	m	$FAT_{50\%}$ (MPa)	$FAT_{97.7\%}$ (MPa)	T_σ (-)
Axial	a_{eff}	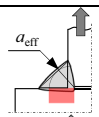	2a	68	39	2.27	2.35	58	30	2.62
	$a+p$	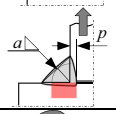	2b	66	39	2.17	2.40	57	31	2.44
Bending	elastic	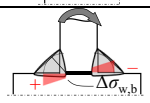	3a	53	38	1.56	2.90	46	33	1.53
	force-pair	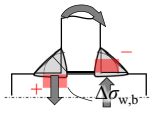	3b	75	53	1.62	2.80	56	39	1.66

Table 2 Chemical composition of the studied materials (wt%)

Material	Type	C	Si	Mn	P	S	Cr	Ni	Mo	Cu	Nb	N
S960 MC	Maximum	0.12	0.25	1.30	0.02	0.01						
	Measured	0.097	0.20	1.09	0.008	0.001	1.13	0.38	0.191	0.033	0.001	0.005
Union X96	Nominal*	0.12	0.8	1.9			0.45	2.35	0.55			

*Undiluted weld metal

Table 3 Mechanical properties of the studied materials

Material	Type	Proof strength $R_{p0.2}$ (MPa)	Ultimate strength R_m (MPa)	Ultimate elongation A (%)	Impact toughness KV (temp.) (J)
S960 MC	Nominal	960	980–1250	7	27 (−40 °C)
	Measured	1041	1210	11	65 (−40 °C)
Union X96	Nominal	930	980	14	80 (+20 °C) 47 (−50 °C)

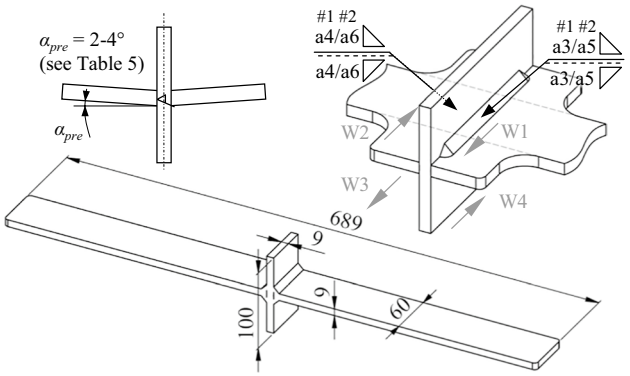

Fig. 4 Shape and dimensions of the test specimens and welding sequence (weld IDs are denoted with "W")

3.2 Specimens

The specimen shape and dimensions have been presented in Fig. 4. To introduce bending stresses, an angular misalignment of 2–4 °C to the transverse plate was applied at both sides. The specimens were prepared using a single-pass robotic GMAW in the horizontal vertical (PB) position [46] with the welding parameters presented in Table 4 and with two different weld throat thicknesses (nominally, $a = 3$ mm and $a = 5$ mm). The welds W1/W4 had slightly lower weld throat thickness than the welds W2/W3 (in both #1 and #2 cases, controlled by adjusting travel speed) in order to produce fatigue failures to this side of the joint (strain gages were attached to this side; see Sect. 3.3). The interpass temperature was less than 50 °C. The weld toes were treated with the high-frequency mechanical impact (HFMI) treatment to improve the weld toe fatigue capacity and thus ensure that the weld root is in the fatigue-critical location of the joints. The run-on and run-off widenings shown in Fig. 4 were sawed, machined, and, eventually, ground to flush before fatigue testing. A total number of 12 specimens were tested, and Table 5 summarizes the test matrix.

3.3 Test setup and measurements

The fatigue tests were carried out using a 150 kN servo-hydraulic fatigue test machine using constant amplitude loading with an applied stress ratio of $R = 0.1$, Fig. 5. To measure the bending effect and straightening of specimens due to the axial loading (geometrically nonlinear behavior), each specimen was equipped with two strain gages positioned at the side W1-W4 at which expected fatigue failure occurs due to the smaller weld throat thickness compared to the side W2-W3. The strain gages (0.6 mm grid size)

Table 4 Welding parameters of the test specimens

Case	a (mm)	Weld ID	Current I (A)	Voltage U (V)	Travel speed v_{travel} (mm/s)	Wire feed rate v_{wire} (m/min)	Heat input Q[1] (kJ/mm)
#1	3	W1, W4	280–290	26.3–26.4	9.5	12.5	0.64
	4	W2, W3	280–290	26.3–26.4	7.0	12.5	0.87
#2	5	W1, W4	280–290	26.3–26.4	6.5	12.5	0.94
	6	W2, W3	280–290	26.3–26.4	5.5	12.5	1.11

[1]In accordance with EN 1011–1 [47] using thermal efficiency factor of 0.8 for GMAW

Table 5 Fatigue test matrix (detailed values for each fatigue test have been presented in Appendix Table 8 and Fig. 12)

Series	Specimen IDs	α_{pre} (°)	Case	a (mm)	DOB = $\frac{\Delta\sigma_b}{\Delta\sigma_m+\Delta\sigma_b}$	n
1	S96_LCX_1–4	2	#1	3	0.25–0.31	4
2	S96_LCX_5–8	4	#1	3	0.55–0.58	4
3	S96_LCX_9–12	2	#2	5	0.18–0.25	4
4	S96_LCX_13–16	4	#2	5	0.34–0.43	4

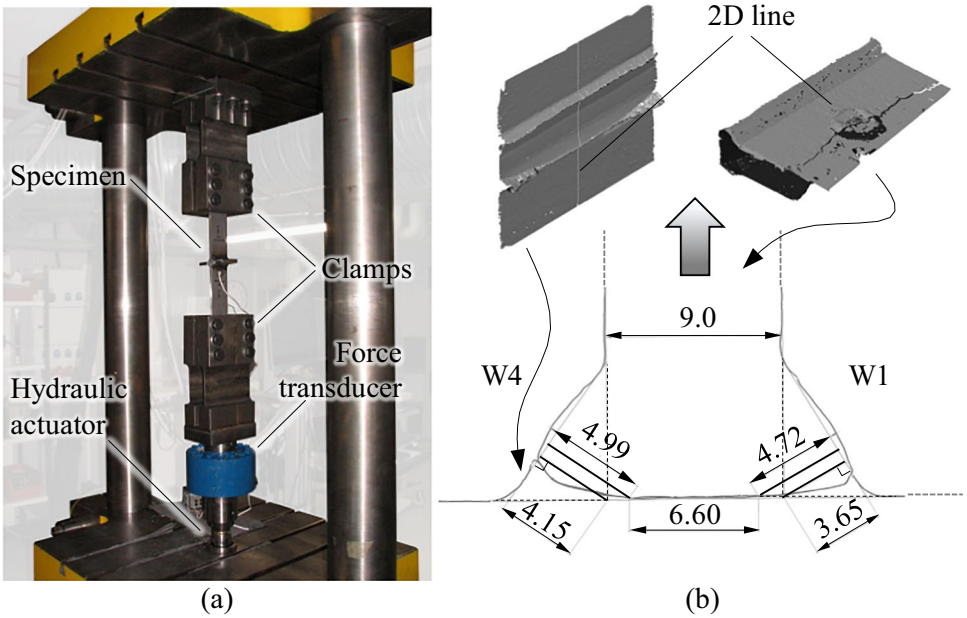

Fig. 5 **a** Fatigue test setup and **b** 3D laser-scanned fractured surfaces with the obtained weld geometries (throat thickness a, effective throat thickness a_{eff}, infusible weld root length w)

were positioned at the hot-spot distance ($0.4t$) from the weld toe.

After the fatigue tests, the weld geometries (a_{eff} and infusible weld root length w) were obtained from the fractured specimens. A Hexagon Romer 3D laser scanning system was applied to determine the point clouds from the fractured surfaces, and the cross-sectional weld geometries were determined, as illustrated in Fig. 5b.

3.4 Results

Figure 6 presents the fatigue test results in terms of the nominal stress system. Results of individual tests have been presented in Appendix Table 8 and Fig. 12. Although robotic GMAW was applied in the preparation of the specimens, minor variation in the resulting DOBs in the tested series was found. The interaction of axial and bending loads is considered by the superposition principle, and the NWSs are calculated as follows:

$$\Delta\sigma_w = \Delta\sigma_{w,m} + \Delta\sigma_{w,b}, \quad (8)$$

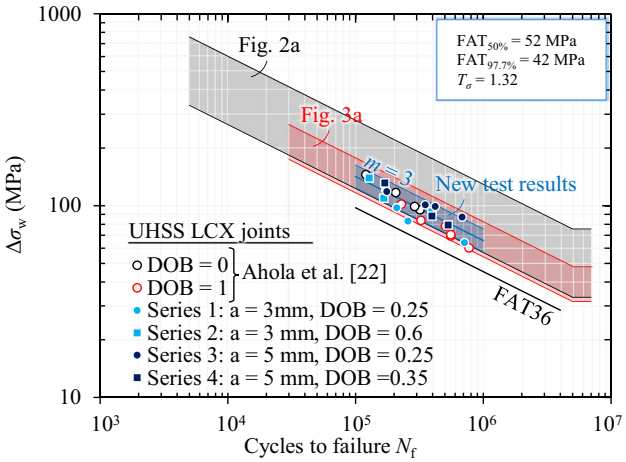

Fig. 6 Fatigue test data plots and results of statistical analysis using NWSs

where $\Delta\sigma_{w,m}$ and $\Delta\sigma_{w,b}$ are calculated based on Eqs. (1) and (6). By using this principle, it can be seen that although at the plate components have high amount of bending stress, the NWSs are dominated by the axial loading — the share of $\Delta\sigma_{w,b}$ from the total NWS $\Delta\sigma_w$ is quite minor, only 15% at

the maximum in the case of DOB = 0.6 (see also the details from Appendix Table 8 and Fig. 12).

4 Numerical analysis

4.1 Finite element modeling

SCFs were determined in the ENS system [27, 48] using the reference radius of $r_{ref} = 1.0$ mm as per the current recommendations. 2D plane strain element models with quadrilateral elements with linear order (124 elements over the 360 °C circumference corresponding to an element size of 0.05 mm in the tangential direction) were employed in the FE analysis [49]. The analyses were carried out using the following:

i) Axial loading (DOB = 0)
ii) Bending loading (DOB = 1)
iii) Combined axial and bending loading corresponding to the loading in the fatigue tests (DOB = 0.18–0.58)

Figure 7 presents a typical FE model used in the analyses. In all cases, 1 MPa unit loading was applied in the model (top fiber stress, $\sigma_{top} = 1$ MPa). The bottom fiber (σ_{bottom}) stress was as follows:

$$\sigma_{bottom} = (1 - 2\mathrm{DOB})\sigma_{top} \tag{9}$$

4.2 Effective notch stress concentrations

Figure 8 presents the results of FE analyses showing the SCF for the axial (DOB = 0), bending (DOB = 1), and combined axial and bending loading in different series. The SCFs, $K_t(r_{ref} = 1.0$ mm), are presented with respect to the top fiber stress at the plate:

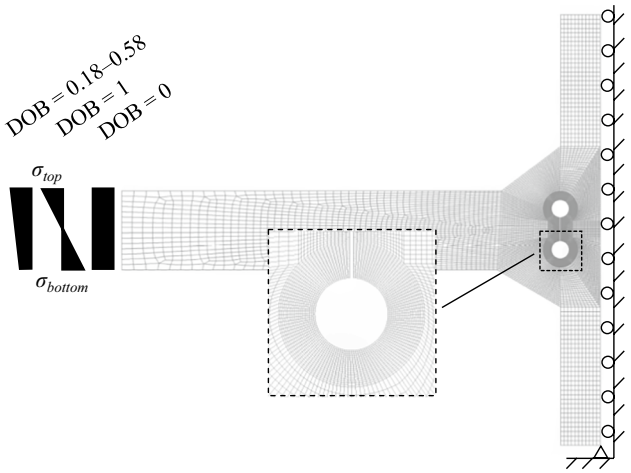

Fig. 7 Finite element model used in the SCF analyses

$$K_t = \frac{\sigma_{ens,root}}{\sigma_{top}}, \tag{10}$$

where $\sigma_{ens,root}$ is the ENS at the weld root, determined from the FE model using maximum principal stress criterion. A clear drop in the SCF was found when the DOB is increased for the evaluated LCX joints with $a_{eff}/t = 0.4$–0.6. Actually, for the DOB = 1, the SCFs are below 1.0, indicating that the crack growth from the weld root failure is not even the critical fatigue failure mechanism. In the present study, the HFMI treatment was employed to increase the fatigue capacity of weld toes, and thus the failures occurred at the weld root and also in the case of high share of bending stress in the series 2. Figure 9 exemplifies the SCF as a function of DOB and indicates the location for the maximum SCF, i.e., $K_{t,max}$.

4.3 Fatigue strength assessments using the effective notch stress system

Employing the SCFs presented in Sect. 5.2, the *S–N* data plots in terms of the ENS system have been presented in Fig. 10. The FAT225 design curve shows unconservative assessment for the LCX joints tested in this study. Meantime, the re-evaluated ENS design curve (FAT168), evaluated in [13] for LCX joints failing from the weld root, shows higher accuracy with the results of this study as the obtained design curve for the joints was $FAT_{97.7\%} = 157$ MPa. The scatter range index was even higher for the ENS system than that of the nominal stress system (see Fig. 6). The results of this study, supported by the findings in [13], indicate that FAT225 does not always provide conservative fatigue assessment for the weld root failures in cruciform joints, and lower FAT class should be used for evaluating root failures.

5 Discussion

The present study investigated the fatigue strength of LCX joints with fillet welds subjected to axial tension, bending, and combined axial and bending loads with DOB = 0.2–0.6 and failing from the weld root. The fatigue test data was extracted from the published literature to statistically evaluate the fatigue strength capacity of these joints under different load configurations employing nominal stress concept and NWSs at the weld section in regard to the recent proposals. Experimental fatigue tests were carried out on the LCX joints made of S960 UHSS grade, continuing the experimental work published in [22]. The specimens were fabricated with the intentionally produced angular misalignment to induce secondary bending stress to the joint and thus investigate the combined axial and bending loads.

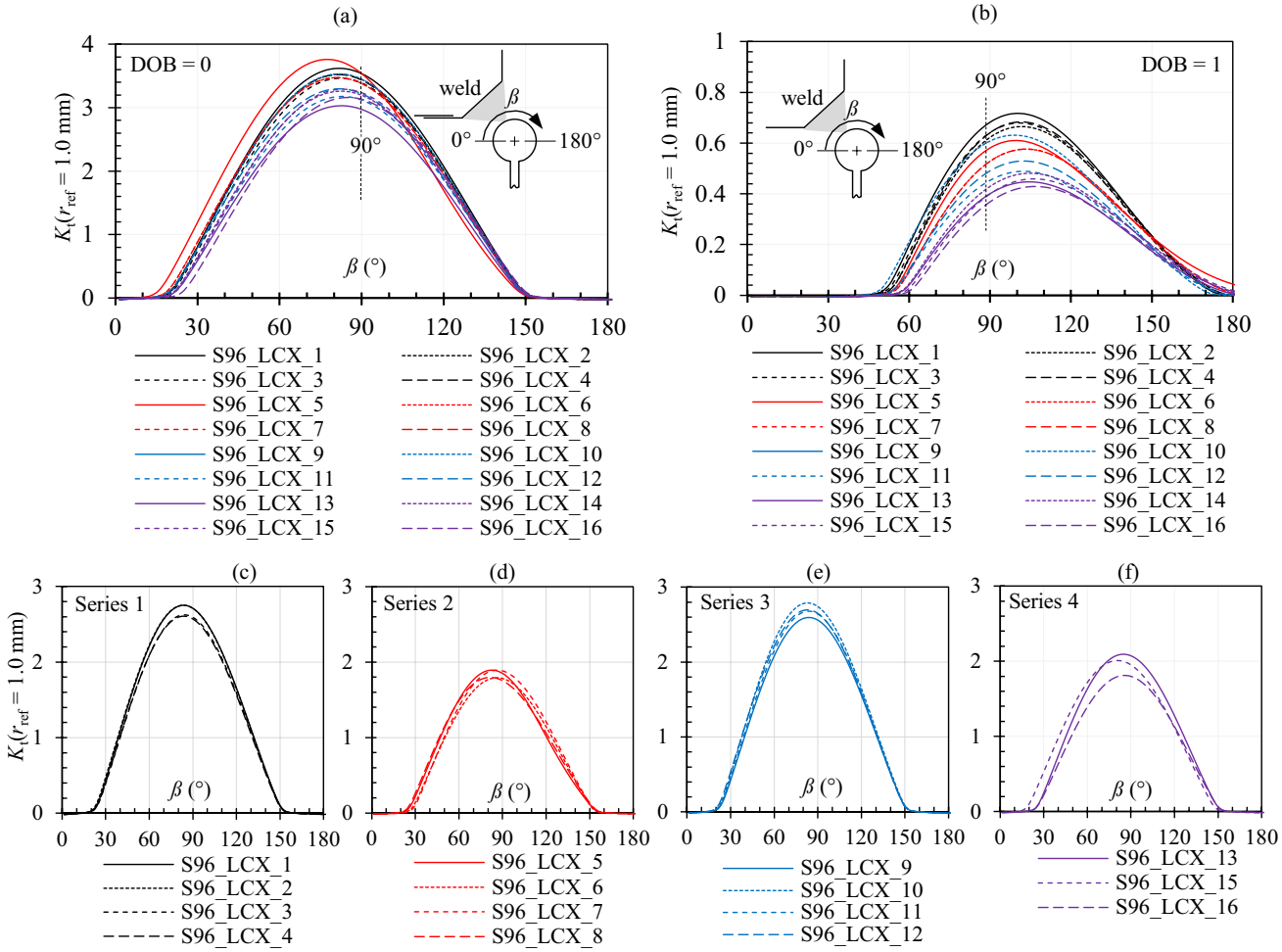

Fig. 8 The SCFs of the ENS along the fictitious notch circumference, $K_t(r_{ref} = 1.0$ mm), for the different cases: **a** DOB = 0, **b** DOB = 1, and **c**–**e** DOB in accordance with the test conditions for series 1–3

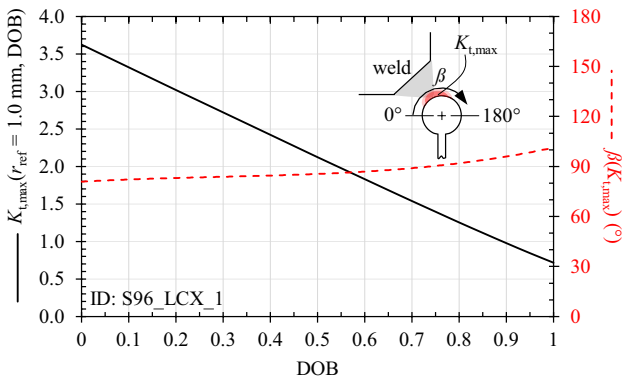

Fig. 9 SCF ($K_{t,max}$) as a function of DOB and the location (angle β) of $K_{t,max}$ along the fictitious notch circumference for the S96_LCX_1 specimen

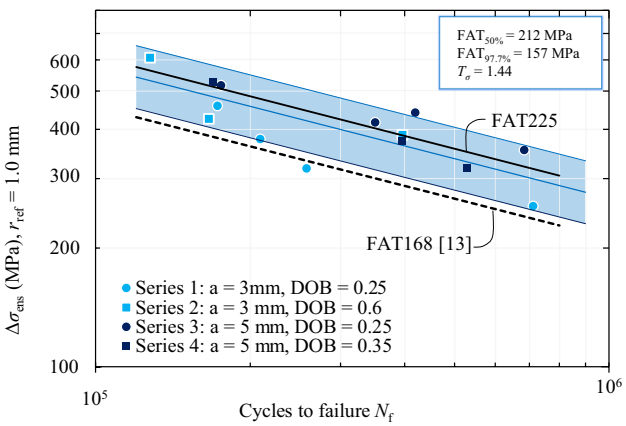

Fig. 10 Fatigue test results in the ENS system

5.1 Fatigue design recommendations for the nominal stress system

The fatigue test data of LCX joints subjected to the axial loading was evaluated employing the nominal stress system, applying effective throat thickness, and external throat thickness summed with weld penetration as a basis for the calculation of NWS at the throat section. The statistical analyses (see Sect. 2.1) revealed that no major difference in the fatigue strength capacity was found ($FAT_{97.7\%} = 38$ MPa for both cases), although 5% lower scatter range was obtained using the NWS calculated on the basis of $a+p$. Due to the limited availability of fatigue test data of LCX joints with weld penetration and failing from the weld root, no further or decisive conclusions can be drawn regarding the most applicable model for calculating NWSs in axially loaded LCX joints. In addition, the free slope parameter for the extracted data was lower than the recommended $m = 3$ (Table 1). A use of steeper slope parameter would decrease the conservatism at the low cycle regime, but on the other hand, $m = 3$ seems to follow the worst fatigue test data points, as it can be seen from Fig. 2. Moreover, the bending test results (Fig. 3 and Table 1) showed slope parameters closer to $m = 3$, and thus equal fixed slope parameter for both axially and bending-loaded joints is justifiable. Further experimental studies should be carried out to evaluate the weld penetration effects on the fatigue strength capacity. However, it is worth mentioning that an increasing weld penetration significantly favors the weld toe failures in LCX joints, as also found in [15].

Based on the statistical analysis of fatigue test data points extracted from the literature, a model in which the NWSs at the throat section are calculated based on the effective throat thickness and assuming linear elastic stress distribution over the joint section is proposed based on this study, different to the model recommended by the EC3 (or the final draft of the new revision [43]). This proposal is based on the three key findings:

- The use of linear elastic stress in the NWSs results in the similar design curve to axially loaded LCX joints, i.e., $FAT_{97.7\%} = 38$ MPa was obtained. These results are also in line with the design curve of FAT36 (or FAT40) recommended currently in the design codes and standards.
- The use of linear elastic stress in the NWSs resulted in slightly lower scatter range index ($T_\sigma = 1.56$) compared to the NWSs calculated based on the force-pair system ($T_\sigma = 1.64$). However, the *S–N* curve analysis was based on the limited number of specimens ($n = 59$), and this finding could be supported by additional fatigue test data.
- The experiments conducted on the LCX joints made of S960 steel grade showed that when using the linear elastic stress distribution, the DOB = 0, DOB = 1, and combined axial and bending tests fall into a same scatter band. This simplifies the fatigue assessments, as different DOBs can be evaluated using a single *S–N* fatigue design curve.

The proposed models were established and verified based on the effective throat thickness. Without groove preparation, no weld penetration is assumed in fatigue design, and Eqs. (6) and (7) receive the following forms (as Eq. (12) originally presented by EC3 revision [43]):

$$\Delta\sigma_{w,b} = \frac{\Delta M c}{I} = \frac{\Delta\sigma_b t^3}{6t^2 a + 12ta^2 + 8a^3}, \tag{11}$$

$$\Delta\sigma_{w,b} = \frac{\Delta F_w}{A} = \frac{\Delta\sigma_b t^2}{6a(a+t)}, \tag{12}$$

In addition to the fatigue test data extracted from the literature, fatigue tests were carried out for the combined axial and bending loading to investigate the interaction loads. The fatigue tests of this study, as well as those tested in the previous study for the same S960 UHSS grade under axial and bending loads (Fig. 6), showed that mean fatigue strength did not reach the mean fatigue strength of the extracted data. In addition, the weld penetration was accurately obtained from the failed specimens, and thus the evaluation NWS is more conservative (giving lower stress ranges) than in the extracted data sets in which the actual weld penetration was approximated based on the given values and macrographs. An increased notch sensitivity for high-strength materials [50] might potentially explain the decrease in the fatigue strength capacity, as the previous experimental works tended to focus on testing mild steels. Nevertheless, the characteristic design curve, FAT36, was still conservative for these results.

5.2 Weld sizing in the interacting axial and bending loads

The results obtained for the pure axial and bending loads indicate that an increasing DOB decreases the fatigue criticality of the weld root in comparison with the weld toe failures. The interaction of axial and bending loading is dominated by the membrane stress, as also indicated by the ENS analyses. An increasing DOB diminishes the SCF at the weld root (when stress at the top fiber is regarded as a reference for the notch stress, see Fig. 9). This observation is in line with the prior study undertaken by Anami et al. [24] in which they found negligibly small effect of 25% increase of bending stress from the membrane stress on the fatigue strength capacity. The ENS concept provided unconservative results when employing the FAT225 design curve and reference radius of $r_{ref} = 1.0$ mm. This finding is in line with the previous works carried out for the LCX joints under axial loading and failing from the weld root [13].

As presented in Fig. 9, an increasing DOB decreases the SCF at the weld root and thus favors fatigue failures originating from the weld toe. To prevent weld root fatigue failures, an important fatigue design step in fillet-welded LCX joints is the weld sizing [13, 15]. Figure 11 presents appropriate throat thickness to plate thickness (a/t) ratios resulting in weld toe and weld root failures when employing the nominal stress and ENS concepts. The color-filled areas describe the region, for both nominal stress and ENS systems, where fatigue failures expectedly occur at the weld root; meanwhile, the unfilled areas describe the region with expected toe failures. In this observation, no weld penetration is considered as per the conventional design assumption [51], i.e., $w = t$. The nominal stress system does not consider the a/t ratio in fatigue assessments (unless FAT40 is employed for $a/t \leq 0.3$ [7]), and thus the computational result is independent of this ratio. FAT36 and FAT63 were considered as the detail categories for the weld root and weld toe failures, respectively. As a result, weld stress range $\Delta\sigma_w$ can be 57% of the top fiber stress. In the ENS concept, computational result is not completely identical for all plate thicknesses (r_{ref}/t ratio varies) — in this observation, a plate thickness of $t = 10$ mm was chosen for the FE analyses. The throat thickness gradually increased from 0.025 to 0.05a/t steps to find the point at which the weld toe and root have identical SCFs. However, it is worth mentioning that the results in Fig. 11 are computationally obtained critical locations for expected failure locations in LCX joints, and further experimental tests should be carried out on cruciform joints with both toe and root failures to verify these findings and applicability of different methods to evaluate the critical location of the joint.

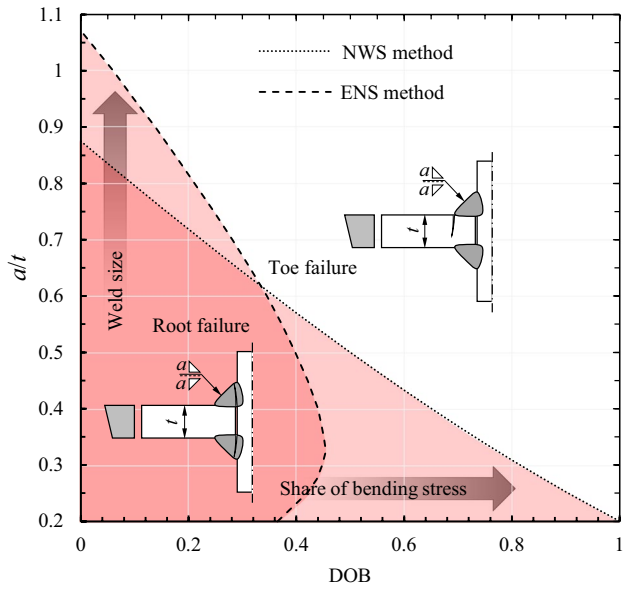

Fig. 11 Critical weld size for the weld toe and weld root failures based on the nominal stress and ENS systems

The results in Fig. 11 confirm the above-discussed aspects related to the root criticality of LCX joints under bending loads. The differences between the ENS and nominal stress systems, particularly with high DOB values, can be explained by the differences in the stress concentrations at the weld toe — the increasing DOB decreases notch SCF at the weld toe due to the symmetric joint configuration, as also found in [52]. Meanwhile, the nominal stress system accounts for the top fiber stress regardless of the DOB, although higher fatigue strength can be expected for the weld toe failures under bending loading [22].

6 Conclusions

The present study investigated the fatigue strength characteristics of LCX joints with fillet welds and failing from the weld root under the axial and bending loading. Experimental fatigue test data was extracted from the literature and supplemented with new experimental tests conducted on the S960 UHSS joints subjected to the combined axial and bending loading. The experimental findings were supported by the numerical analyses employing the ENS concept to evaluate weld root capacity. Based on the results and subsequent analyses, the following conclusions can be drawn.

- In the nominal stress system, a use of linear elastic stress distribution over the joint section in bending resulted in the agreement with the characteristic design curve for the axially loaded LCX joints and current design recommendations, i.e., FAT36 provides feasible results in fatigue assessments without overconservatism. When assuming force-pair system (which is under consideration by the working group revising EC3), higher fatigue class should be used for bending loads to avoid redundant conservatism in fatigue assessments. The results obtained using the force-pair system provided a good agreement with the axial data in terms of the mean fatigue strength capacity but resulted in a higher characteristic design curve ($FAT_{97.7\%} = 54$ MPa) than the FAT36 detail category for the weld root failures.
- In general, bending loading has negligibly low effect of the weld stresses in the joints with the combined axial and bending loading. Consequently, consideration of bending stresses does not play a major role in the fatigue assessment of such joints. In the bending-loaded LCX joints with low a/t or a_{eff}/t ratios, or in the joints enhanced with the post-weld treatments, however, the weld root capacity can be an important fatigue design criteria, and this study proposed a model for assessing fatigue strength of such joints.
- The ENS concept with the FAT225 characteristic design curve does not provide conservative assessment for the weld root failures in LCX joints.

Appendix 1 Details for the extracted fatigue test data series

Table 6 Fatigue test data series for axially loaded (A) joints

Ref		f_y /$R_{p0.2}$ (MPa)		t (mm)	a_{eff} /t	R	Process[1]
	Loading type	Base material	Filler				
[40]	A	315	[2]	16	0.35	0.4	GMAW
[40]	A	315	[2]	16	0.48	0.4	GMAW
[40]	A	315	[2]	16	0.47	0.4	GMAW
[40]	A	315	[2]	16	0.59	0.4	GMAW
[40]	A	315	[2]	16	0.38	0.4	GMAW
[41]	A	413	485	9	0.53	0	SMAW
[41]	A	397	485	20	0.48	0	SMAW
[42]	A	315	510	16	0.53	0	GMAW
[42]	A	315	510	16	0.53	0.75	GMAW
[4]	A	693	[2]	12	0.46	0.1	[2]
[4]	A	693	[2]	12	0.45	0.1	[2]
[4]	A	693	[2]	12	0.41	0.1	[2]
[4]	A	693	[2]	12	0.52	0.1	[2]
[4]	A	693	[2]	12	0.41	0.1	[2]
[4]	A	693	[2]	12	0.36	0.1	[2]
[24]	A	325	[2]	22	0.32	0	GMAW
[24]	A	325	[2]	22	0.5	0	GMAW
[30]	A	292	[2]	16	0.37	0	Laser-GMAW
[31]	A	356	460	10	0.55	0	FCAW
[31]	A	356	460	10	0.55	0.5	FCAW
[31]	A	595	550	10	0.64	0	FCAW
[32]	A	345	[2]	12	0.56	0.1	MCAW
[33]	A	392	565	28	0.29	0.05	GMAW
[33]	A	392	494	28	0.36	0.05	GMAW
[33]	A	554	491	24	0.35	0.05	GMAW
[12]	A	362	[2]	15	0.28	0.5–0.75	FCAW
[12]	A	362	[2]	15	0.38	0.5–0.75	FCAW
[34]	A	534	407	16	0.45	0.05	GMAW
[34]	A	534	665	16	0.42	0.05	GMAW
[34]	A	534	407	16	0.66	0.05	GMAW
[34]	A	534	665	16	0.5	0.05	GMAW
[34]	A	534	407	16	0.71	0.05	GMAW
[34]	A	534	665	16	0.65	0.05	GMAW
[35]	A	306	[2]	16	0.4	0.1	SMAW
[36]	A	744	[2]	16	0.56	0.2	GMAW
[37]	A	395	530	14	0.43	0.5	GMAW
[17]	A	345	[2]	10	0.5	0.1	SMAW
[3]	A	297	425	6	0.33	0	GTAW
[3]	A	297	425	6	0.48	0	GTAW
[3]	A	297	425	6	0.55	0	GTAW
[3]	A	297	425	6	0.62	0	GTAW
[38]	A	250	[2]	10	0.71	0	[2]
[39]	A	1100	930	9	0.52	0.1	GMAW
[22]	A	960	930	8	0.5	0.1	GMAW
[5]	A	370	[2]	8	0.71	0.5	[2]

[1]Gas metal arc welding (GMAW), shield metal arc welding (SMAW), flux-cored arc welding (FCAW), gas tungsten arc welding (GTAW). [2]Not specified/given

Table 7 Fatigue test data series for bending-loaded joints

Ref	Loading type[1]	f_y /$R_{p0.2}$ (MPa)		t (mm)	a_{eff}/t	R	Process
		Base material	Filler				
[11, 12]	4B	362	[2]	18	0.21	0.5–0.8	FCAW
[11, 12]	4B	362	[2]	18	0.27	0.5–0.8	FCAW
[10]	3B	620	765	33	0.44	0.1	GTAW
[10]	3B	620	765	33	0.35	0.1	GTAW
[10]	3B	620	395	33	0.35	0.1	GTAW
[22]	4B	960	980	9	0.5	0.1	GMAW
[23]	[2]	264	300	16	0.28	0	SMAW
[23]	[2]	240	300	32	0.26	0	SMAW
[23]	[2]	264	300	16	0.26	0	SMAW
[23]	[2]	240	300	32	0.33	0	SMAW

[1]Three-point bending (3B), four-point bending (4B). [2]Not specified/given

Appendix 2 Results of the experimental fatigue tests

Table 8 Fatigue test data points

ID	$a_{eff,W1}$ (mm)	$a_{eff,W4}$ (mm)	w (mm)	ΔF (kN)	$\Delta\sigma_m$ (MPa)	$\Delta\sigma_{m,w}$ (MPa)	$\Delta\sigma_b$ (MPa)	$\Delta\sigma_{b,w}$ (MPa)	$\Delta\sigma_w$ (MPa)	N_f (cycles)
S96_LCX_1	4.7	4.8	6.7	45.0	83.3	78.4	34	4.6	82.9	257,820
S96_LCX_2	4.7	5.0	6.6	54.0	100.0	92.7	35	4.6	97.3	209,323
S96_LCX_3	5.0	4.9	6.3	67.5	125.0	113.8	50	6.4	120.2	172,766
S96_LCX_4	4.9	5.0	6.4	36.0	66.7	60.2	29	3.7	63.9	712,009
S96_LCX_5	4.5	5.1	6.9	45.0	83.3	78.0	109	14.6	92.5	396,423
S96_LCX_6[1]	5.4	5.5	7.2	36.0	66.7	55.0	86	9.0	64.0	433,679
S96_LCX_7	4.7	5.0	6.8	67.5	125.0	116.2	172	22.8	139.0	127,717
S96_LCX_8	4.7	5.0	7.1	54.0	100.0	92.9	122	16.1	108.9	166,218
S96_LCX_9	5.8	5.8	6.8	67.5	125.0	97.2	38	3.5	100.8	350,642
S96_LCX_10	5.4	5.4	7.4	54.0	100.0	83.3	33	3.5	86.8	684,011
S96_LCX_11[2]	6.3	6.1	6.9	85.5	158.3	115.1	35	2.8	117.9	175,737
S96_LCX_12	5.3	5.8	7.2	63.0	116.7	94.4	43	4.3	98.8	419,363
S96_LCX_13	6.3	6.4	6.2	63.0	117	83.2	62	4.8	88.0	395,378
S96_LCX_14[3]	5.8	5.6	6.6	72.0	133.3	105.7	0	0	105.7	333,382
S96_LCX_15	5.7	5.8	6.8	85.5	158.3	123.3	82	7.7	130.9	169,437
S96_LCX_16	6.2	6.1	6.0	54.0	100	72.87	76	6.2	79.0	529,913

[1]Unsuccesful fatigue test, error in welding preparation (not included in the analyses). [2]Failure from the side W2-W3 (geometries for these welds). [3]Unsuccesful fatigue test, error in welding preparation (DOB = 0)

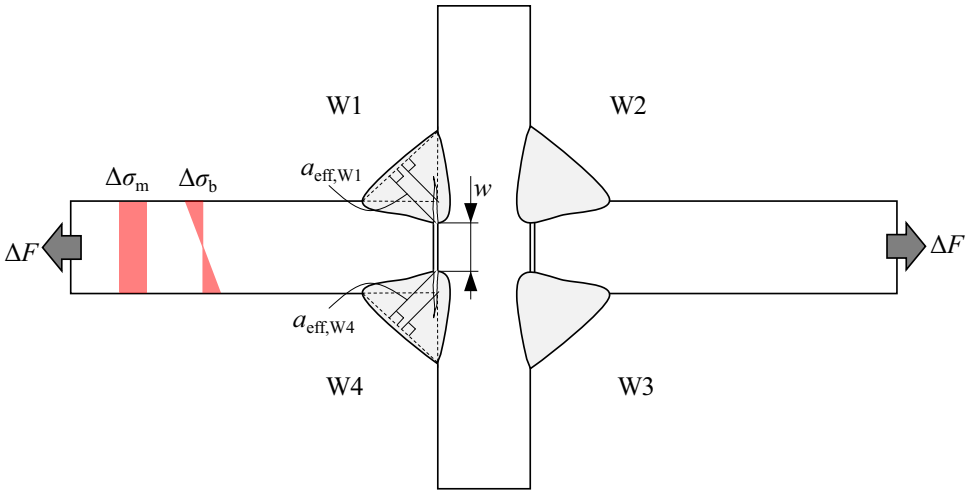

Fig. 12 Description of symbols in Table 8

Author contribution AA — conceptualization, formal analysis, funding acquisition, investigation, methodology, validation, visualization, and writing — original draft; HRR — investigation and resources; TB — conceptualization, supervision, and funding acquisition; OK — formal analysis, methodology, and resources.

Funding Open Access funding provided by LUT University (previously Lappeenranta University of Technology (LUT)). The authors wish to thank Business Finland for the funding of experiments in the Intelligent Steel Applications (ISA) project, and the corresponding author gratefully acknowledge Jenny and Antti Wihuri Foundation for their financial support to conduct the research work and analyses.

Data availability Appendices 1 and 2 provide the details of fatigue test data applied in this work. Further necessary information can be acquired by contacting the corresponding author.

Declarations

Conflict of interest The authors declare no competing interests.

References

1. Xing S, Dong P, Wang P (2017) A quantitative weld sizing criterion for fatigue design of load-carrying fillet-welded connections. Int J Fatigue 101:448–458. https://doi.org/10.1016/j.ijfatigue.2017.01.003
2. Cui C, Zhang Q, Bao Y et al (2018) Fatigue performance and evaluation of welded joints in steel truss bridges. J Constr Steel Res 148:450–456. https://doi.org/10.1016/j.jcsr.2018.06.014
3. Singh PJ, Achar DRG, Guha B, Nordberg H (2002) Fatigue life prediction of gas tungsten arc welded AISI 304L cruciform joints with different LOP sizes. Int J Fatigue 25:1–7. https://doi.org/10.1016/S0142-1123(02)00067-1
4. Song W, Liu X, Razavi SMJ (2018) Fatigue assessment of steel load-carrying cruciform welded joints by means of local approaches. Fatigue Fract Eng Mater Struct 1–16. https://doi.org/10.1111/ffe.12870
5. Jakubczak H, Glinka G (1986) Fatigue analysis of manufacturing defects in weldments. Int J Fatigue 8:51–57. https://doi.org/10.1016/0142-1123(86)90053-8
6. EN 1993–1–9 (2005) Eurocode 3: design of steel structures - part 1–9: fatigue
7. Hobbacher A (2016) Recommendations for fatigue design of welded joints and components, 2nd edn. Springer International Publishing, Cham
8. BS7608:2014 +A1:2015 (2015) Guide to fatigue design and assessment of steel products. British Standards Institution
9. DNVGL-RP-C203 (2016) Fatigue design of offshore steel structures. Det Norske Veritas - Germanischer Lloyd
10. Ghafoori-Ahangar R, Verreman Y (2019) Fatigue behavior of load-carrying cruciform joints with partial penetration fillet welds under three-point bending. Eng Fract Mech 215:211–223. https://doi.org/10.1016/j.engfracmech.2019.05.015
11. Mori T (2009) Assessment of fatigue strength of cruciform welded joints failing from weld roots under out-of-plane bending. IIW-document XIII-2287–09
12. Mori T, Uchida D, Fukuoka T, Myoken M (2010) Assessment of fatigue strength of cruciform welded joints failing from weld roots under out-of-plane bending (in Japanese). Japanese Soc Steel Constr 66:568–575. https://doi.org/10.2208/jsceja.66.568
13. Rohani Raftar H, Dabiri M, Ahola A, Björk T (2021) Re-evaluation of weld root fatigue strength for load-carrying fillet welded joints using the notch stress concept. Int J Fatigue 144:106076. https://doi.org/10.1016/j.ijfatigue.2020.106076
14. RohaniRaftar H, Dabiri E, Ahola A, Björk T (2021) Weld root fatigue assessment of load-carrying fillet welded joints: 4R method compared to other methods. Int J Fatigue 156:106623
15. Bartsch H, Feldmann M (2021) Numerical and databased investigations on the fatigue of cruciform joints with gaps. J Constr Steel Res 185:106843. https://doi.org/10.1016/j.jcsr.2021.106843
16. Fricke W, Kahl A, Paetzold H (2006) Fatigue assessment of root cracking of fillet welds subject to throat bending using the structural stress approach fatigue assessment of root cracking of fillet welds subject to throat bending using the structural stress

approach for structural stress. Weld World 50:64–74. https://doi.org/10.1007/BF03266538
17. Sørensen JD, Tychsen J, Andersen JU, Brandstrup RD (2006) Fatigue analysis of load-carrying fillet welds. J Offshore Mech Arct Eng 128:65. https://doi.org/10.1115/1.2163876
18. Braun M, Milaković AS, Renken F et al (2020) Application of local approaches to the assessment of fatigue test results obtained for welded joints at sub-zero temperatures. Int J Fatigue 138:105672. https://doi.org/10.1016/j.ijfatigue.2020.105672
19. Meneghetti G, Lazzarin P (2013) The peak stress method for fatigue strength assessment of tube-to-flange welded joints under torsion loading. Weld World 57:265–275. https://doi.org/10.1007/s40194-013-0022-x
20. Foti P, Santonocito D, Risitano G, Berto F (2021) Fatigue assessment of cruciform joints: comparison between strain energy density predictions and current standards and recommendations. Eng Struct 230:111708. https://doi.org/10.1016/j.engstruct.2020.111708
21. Baumgartner J, Schmidt H, Ince E et al (2015) Fatigue assessment of welded joints using stress averaging and critical distance approaches. Weld World 59:731–742. https://doi.org/10.1007/s40194-015-0248-x
22. Ahola A, Björk T, Barsoum Z (2019) Fatigue strength capacity of load-carrying fillet welds on ultra-high-strength steel plates subjected to out-of-plane bending. Eng Struct 196:109282. https://doi.org/10.1016/j.engstruct.2019.109282
23. Ouchida H, Nishioka A (1964) A study of fatigue strength of fillet welded joints. Hitachi Rev 3–14
24. Anami K, Yokota H, Takao R (2008) Evaluation of fatigue strength of load-carrying cruciform welded joint under combination of axial loading and out-of-plane bending. Int J Steel Struct 8:183–188
25. Ahola A (2020) Stress components and local effects in the fatigue strength assessment of fillet weld joints made of ultra-high-strength steels. Doctoral dissertation, LUT University. Accessible: http://urn.fi/URN:ISBN:978-952-335-595-8. Accessed 20 June 2021
26. Fricke W (2012) IIW Recommendations for the fatigue assessment of welded structures by notch stress analysis. Woodhead Publishing
27. Sonsino CM, Fricke W, De Bruyne F et al (2012) Notch stress concepts for the fatigue assessment of welded joints - background and applications. Int J Fatigue 34:2–16. https://doi.org/10.1016/j.ijfatigue.2010.04.011
28. Kang W, Kim WS, Paik YM (2002) Fatigue strength of fillet welded steel structure under out-of-plane bending. Int J Korean Weld Soc 2:33–39
29. Maddox SJ (2015) Allowance for bending in fatigue design rules for welded joints. IIW-document XIII 2580-15
30. Hanji T, Tateishi K, Shimizu M et al (2019) Fatigue strength of cruciform joints and longitudinal joints with laser-arc hybrid welding. Weld World 63:1379–1390. https://doi.org/10.1007/s40194-019-00745-w
31. Braun M, Scheffer R, Fricke W, Ehlers S (2020) Fatigue strength of fillet-welded joints at subzero temperatures. Fatigue Fract Eng Mater Struct 43:403–416. https://doi.org/10.1111/ffe.13163
32. Zong L, Shi G, Wang Y-Q et al (2017) Investigation on fatigue behaviour of load-carrying fillet welded joints based on mix-mode crack propagation analysis. Arch Civ Mech Eng 17:677–686. https://doi.org/10.1016/j.acme.2017.01.009
33. Hanji T, Miki C, Saiprasertkit K (2012) Low- and high-cycle fatigue behaviour of load-carrying cruciform joints containing incomplete penetration and strength mismatch. Weld World 56:133–146. https://doi.org/10.1007/BF03321357
34. Saiprasertkit K, Hanji T, Miki C (2012) Fatigue strength assessment of load-carrying cruciform joints with material mismatching in low- and high-cycle fatigue regions based on the effective notch concept. Int J Fatigue 40:120–128. https://doi.org/10.1016/j.ijfatigue.2011.12.016
35. Vishnuvardhan S, Raghava G, Saravanan M, Gandhi P (2016) Fatigue life evaluation of fillet welded cruciform joints with load-carrying welds. Trans Indian Inst Met 69:585–589. https://doi.org/10.1007/s12666-015-0822-3
36. Frank KH (1971) The fatigue strength of fillet welded connections. Doctoral dissertation, Lehigh University
37. Kainuma S, Kim I-T (2005) Fatigue strength evaluation of load-carrying cruciform fillet-welded joints made with mild steel plates of different thickness. Int J Fatigue 27:810–816. https://doi.org/10.1016/j.ijfatigue.2005.01.002
38. Yamaguchi I, Terada Y, Nitta A (1968) On the fatigue strength of steels for ship structure. J Soc Nav Archit Japan 1:19–35
39. Ahola A, Skriko T, Björk T (2019) Experimental investigation on the fatigue strength assessment of welded joints made of S1100 ultra-high-strength steel in as-welded and post-weld treated condition. In: Zingoni A (ed) Proc. 7th Int. Conf. Struct. Eng. Mech. Comput. (SEMC 2019). Cape Town, South Africa, 2–4 Sept. 2019. pp 1254–1259
40. Kainuma S, Mori T (2006) A fatigue strength evaluation method for load-carrying fillet welded cruciform joints. Int J Fatigue 28:864–872. https://doi.org/10.1016/j.ijfatigue.2005.10.004
41. National Research Institute for Metals (1980) Fatigue data sheet, no. 18: data sheets on fatigue properties for load-carrying cruciform welded joints of SM50B rolled steel for welded structure
42. Kainuma S, Mori T (2008) A study on fatigue crack initiation point of load-carrying fillet welded cruciform joints. Int J Fatigue 30:1669–1677. https://doi.org/10.1016/j.ijfatigue.2007.11.003
43. prEN 1993–1–9 (2020) Final draft of Eurocode 3 - design of structures - part 1–9: fatigue. European Committee for Standardization
44. Amraei M, Ahola A, Afkhami S et al (2019) Effects of heat input on the mechanical properties of butt-welded high and ultra-high strength steels. Eng Struct. https://doi.org/10.1016/j.engstruct.2019.109460
45. Björk T, Ahola A, Tuominen N (2018) On the design of fillet welds made of ultra-high strength steel. Weld World 62:985–995. https://doi.org/10.1007/s40194-018-0624-4
46. EN ISO 6947 (2019) Welding and allied processes. Welding positions (International Organization for Standardization 6947:2019). 23
47. EN 1011–1 (2009) Welding - recommendations for welding of metallic materials - part 1: general quidance for arc welding. European Committee for Standardization
48. Fricke W (2012) IIW Recommendations for the Fatigue Assessment of Welded Structures by Notch Stress Analysis. Woodhead Publishing Ltd. ISBN 978-0-85709-855-9
49. Baumgartner J, Bruder T (2013) An efficient meshing approach for the calculation of notch stresses. Weld World 57:137–145. https://doi.org/10.1007/s40194-012-0005-3
50. Dowling NE (2006) Mechanical behavior of materials. Engineering methods for deformation, fracture, and fatigue. Prentice Hall: Pearson
51. EN 1993–1–8 (2005) Eurocode 3: design of steel structures - part 1–8: design of joints. European Committee for Standardization
52. Ahola A, Nykänen T, Björk T (2017) Effect of loading type on the fatigue strength of asymmetric and symmetric transverse non-load carrying attachments. Fatigue Fract Eng Mater Struct 40:670–682. https://doi.org/10.1111/ffe.12531